PHYSICAL REVIEW B **96**, 014303 (2017)

Quantum correlations at infinite temperature: The dynamical Nagaoka effect

Márton Kanász-Nagy,[1,*] Izabella Lovas,[2] Fabian Grusdt,[1] Daniel Greif,[1] Markus Greiner,[1] and Eugene A. Demler[1]

[1]*Department of Physics, Harvard University, Cambridge, Massachusetts 02138, USA*

[2]*MTA-BME Exotic Quantum Phases "Momentum" Research Group and Department of Theoretical Physics, Budapest University of Technology and Economics, 1111 Budapest, Hungary*

(Received 10 May 2017; published 14 July 2017)

Do quantum correlations play a role in high-temperature dynamics of many-body systems? A common expectation is that thermal fluctuations lead to fast decoherence and make dynamics classical. In this paper we provide a striking example that a single particle created in a featureless, infinite temperature spin bath not only exhibits nonclassical dynamics but it also induces strong long-lived correlations between the surrounding spins. We study the nonequilibrium dynamics of a hole created in a Mott insulator in the atomic limit, which corresponds to a degenerate spin system. In the absence of interactions, the spin correlations arise purely from quantum interference. Furthermore, these correlations are both antiferromagnetic and ferromagnetic, in striking contrast to the equilibrium Nagaoka effect. These results are relevant for a number of condensed matter spin systems and should be observable using state of the art bosonic or fermionic quantum gas microscopes.

DOI: 10.1103/PhysRevB.96.014303

I. INTRODUCTION

Understanding the role of quantum coherence in dynamics of many-body systems at high temperatures remains a challenging open problem. Usually coherence is fragile and quickly destroyed by interaction with the environment and by local fluctuations inherent to thermal ensembles. Hence it is commonly assumed that observing quantum coherent dynamics requires preparing isolated quantum systems close to their ground states. Famous experimental demonstrations of quantum coherence, including interference of Cooper pairs in nanostructures [1,2] or interference of atomic Bose-Einstein condensates and superfluids [3–5], have all been achieved under these conditions. On the other hand, it has been argued that quantum interference can lead to strong deviations from simple classical dynamics. For example, the breakdown of spin diffusion was predicted for the Heisenberg model even at infinite temperature [6–8]. Several important examples can be found in biophysics: in photosynthesis the interplay of quantum interference and decoherence leads to a much faster energy transport than would be possible classically [9–11]; quantum coherence has also been suggested to play a crucial role in bird navigation [12] and the chemistry of smelling [13]. Understanding how quantum interference can operate at high temperatures is therefore a crucial question, with tremendous potential for quantum information science [14–16], condensed matter [17], and biology [18].

Whereas it is well understood that the entanglement of a subsystem with its environment leads to dephasing that drives the subsystem towards classical behavior, the fate of quantum coherence created in the environment is much less discussed. It is conventionally assumed that the environment's coherence quickly vanishes due to dephasing among its large number of degrees of freedom [19]. Here we show however that this is not necessarily the case. We present a surprising example, where adding a single quantum particle to an infinite temperature spin environment can lead to appreciable dynamical correlations among the spins (Fig. 1). We consider a system of noninteracting spins on a two-dimensional lattice, which is routinely realizable with bosonic or fermionic ultracold quantum gas microscopes. In a deep optical lattice, on-site repulsion brings the atoms into a Mott state, where each site is occupied by exactly one atom. The spins are represented by internal degrees of freedom of the atoms, such as their hyperfine states [20] or nuclear spins [21], with $\mathcal{N} = 2S + 1$ degrees of freedom, modeling a spin S system. In the limit of strong on-site repulsion, the spins completely decouple, as virtual tunneling to the neighboring sites is suppressed. This realizes the noninteracting spin system discussed here. Removing a spin on one site creates a hole that can move on the lattice at no energy cost and permute the spins during its motion [22–25], see Figs. 1(a) and 1(b). In contrast to a classical particle performing Brownian motion that would only scramble the random spins along its path and keep the environment completely disordered, the quantum mechanical hole is capable of exploring alternative paths in parallel. As each path can lead to different permutations of the spins, the superposition of these outcomes creates entanglement in the spin bath. This leads to dynamical spin correlations in the environment, whereas individual sites remain paramagnetic. In contrast to the usual polaron effect, where a particle locally modifies its environment due to their interaction [26–34], these correlations arise purely from quantum interference.

Our system is also closely related to the ideas of dissipationless decoherence [35,36], studied in the context of quantum information [15,16], condensed matter [37], and cosmology [38]. Even though there is no energy transfer between the hole and the environment, the hole's propagation is slowed down as quantum coherence is suppressed due to its entanglement with the surrounding spins as was studied by Carlström *et al.* [25]. The new insight of our work is that this process also induces spin correlations in the environment (Figs. 1 and 2), and therefore these correlations and decoherence are intimately related. The noninteracting system discussed here is special in the sense that the degrees of freedom in the environment are all degenerate, which suppresses the effects of dephasing. In fact, during the time scale of our simulations, these correlations remain finite.

*mkanasznagy@fas.harvard.edu

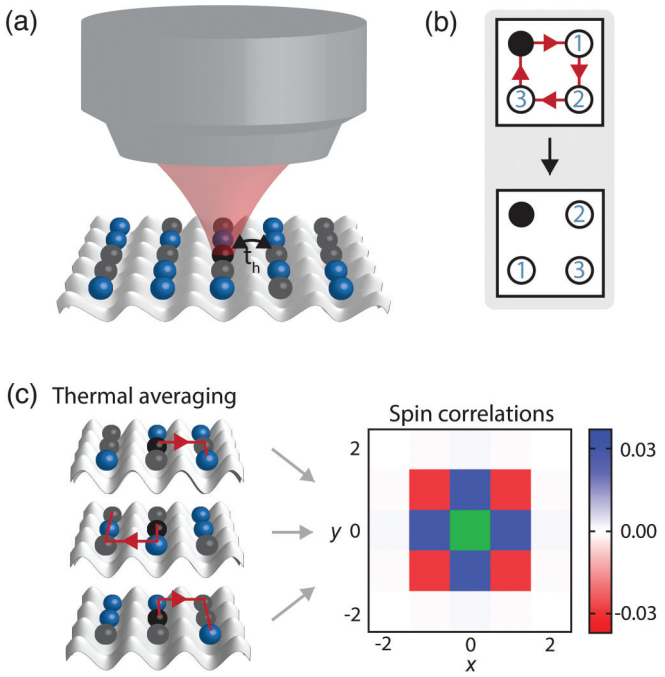

FIG. 1. Experimental realization of the proposed procedure. (a) The system of noninteracting spins is realized by creating a Mott insulator of spinful atoms in a deep optical lattice. The atoms are shown as gray (dark) and blue (light) dots. In the limit of infinitely strong on-site repulsion, the spin interaction vanishes. The hole (black) is created at the beginning of the experiment by removing one of the atoms; its position and the spin correlations in the environment can be measured after a propagation time t using a quantum gas microscope. (b) As the hole moves along the trajectory indicated by arrows (top) the spins on this path are reordered (bottom). (c) Spin correlations are calculated by thermal averaging over all possible spin configurations. During its dynamics, the hole explores all alternative paths simultaneously. Due to its interplay with the spins, the hole permutes each of these environments differently, leading to nonvanishing spin correlations even after thermal averaging. Right panel: Spin correlations C_{ol} in the laboratory frame between the origin o (green site at the center) and site l, whose coordinates are denoted by x and y. The calculations were performed at time $t = 1.1$ in a spin $S = 1/2$ environment.

We identify the interference terms that make the hole's dynamics dependent on the environment's spin S [25]. These terms are identical to those that generate spin correlations in the environment, and they vanish exponentially in environments of large spin. Finally, we find that the simple analytical model of a hole on the Bethe lattice [39] closely approximates the hole's dynamics in a $S \to \infty$ environment within the time scales of the simulation. It has been suggested that the dynamics of the hole should crossover from the initial ballistic to diffusive behavior at long times [25]. However, this question remained inconclusive due to the limited time available for numerical simulations. The correspondence with the Bethe lattice provides further evidence that the hole's dynamics indeed crosses over to diffusive behavior.

Dynamics of charge carriers in fluctuating and disordered spin background lies at the heart of many physical systems, including high-temperature superconductors [24,40,41], the paramagnetic phase of supersolid ^{3}He [42–45], organic materials [46], manganites exhibiting colossal magneto resistance effect [47,48], and multicomponent ultracold atoms in optical lattices [20,49,50]. The Hubbard model provides a paradigmatic model of these systems, characterized by the nearest neighbor tunneling energy t_h and an on-site repulsion between the atoms. As the spinful atoms or electrons in each of these systems repel each other strongly, they occupy individual lattice sites, realizing a Mott insulator of spins [20,24,49,50]. Assuming spin-independent on-site repulsion U, a spin interaction J of the order of t_h^2/U is provided by virtual tunneling to neighboring sites, leading to the so-called t-J model [24]. The spin coupling J then vanishes in the limit of large on-site interactions $U \to \infty$, realizing the noninteracting spin system studied here.

Despite its simplicity, the degenerate spin environment has surprisingly rich physics. As has been shown by Nagaoka [22,23], the ground state of the system becomes ferromagnetically ordered in the presence of a single hole, as this state provides free propagation to the hole so that it can minimize its kinetic energy. Here we discuss the opposite limit of an infinite temperature spin environment, where the hole creates dynamical correlations among the spins. These correlations are of similar origin as the equilibrium Nagaoka effect, as they arise from the dependence of the hole's dynamics on the surrounding spin configurations: locally ferromagnetic spin domains lead to enhanced quantum coherence and to faster propagation. As the hole acts on the spins in each spin background differently, the resulting correlations are not averaged out to zero due to thermal fluctuations. However, in contrast to the Nagaoka ground state, the correlations studied in this paper are both ferromagnetic and antiferromagnetic.

II. EXPERIMENTAL REALIZATION

Figure 1(a) shows a possible experimental realization of our proposal. The noninteracting spin system is realized by creating a Mott insulator of fermionic or bosonic atoms in a deep optical lattice, with a single atom per site. Tuning the lattice depth allows one to reach the limit of strong on-site repulsion $U \gg t_\mathrm{h}$ such that the spin interactions become negligible. The hole can be created by removing a single atom at the origin o, with coordinates (0,0), using a quantum gas microscope that can optically address sites independently [51]. The microscope can also measure the hole's position as well as the spin state at each site after a propagation time t. In order to account for thermal fluctuations at infinite temperature, this procedure has to be repeated many times, in each case with a different, random initial spin configuration (see Appendix A), resulting in an averaging over all possible spin states, as we show in Fig. 1(c).

The dynamics of the hole is governed by the Hamiltonian

$$\hat{H} = -t_\mathrm{h} \sum_{\langle jl \rangle} \hat{c}_j^\dagger \hat{\mathcal{P}}_{jl} \hat{c}_l,$$

where the operator $\hat{c}_l$ annihilates the hole at site l. As the hole moves from site l to j, the operator $\hat{\mathcal{P}}_{jl}$ moves the spin at site j to site l. Since there is no energy cost of moving the spins around, the tunneling t_h is the single energy scale of the model, and it is chosen to be $t_\mathrm{h} \equiv 1$, which also determines

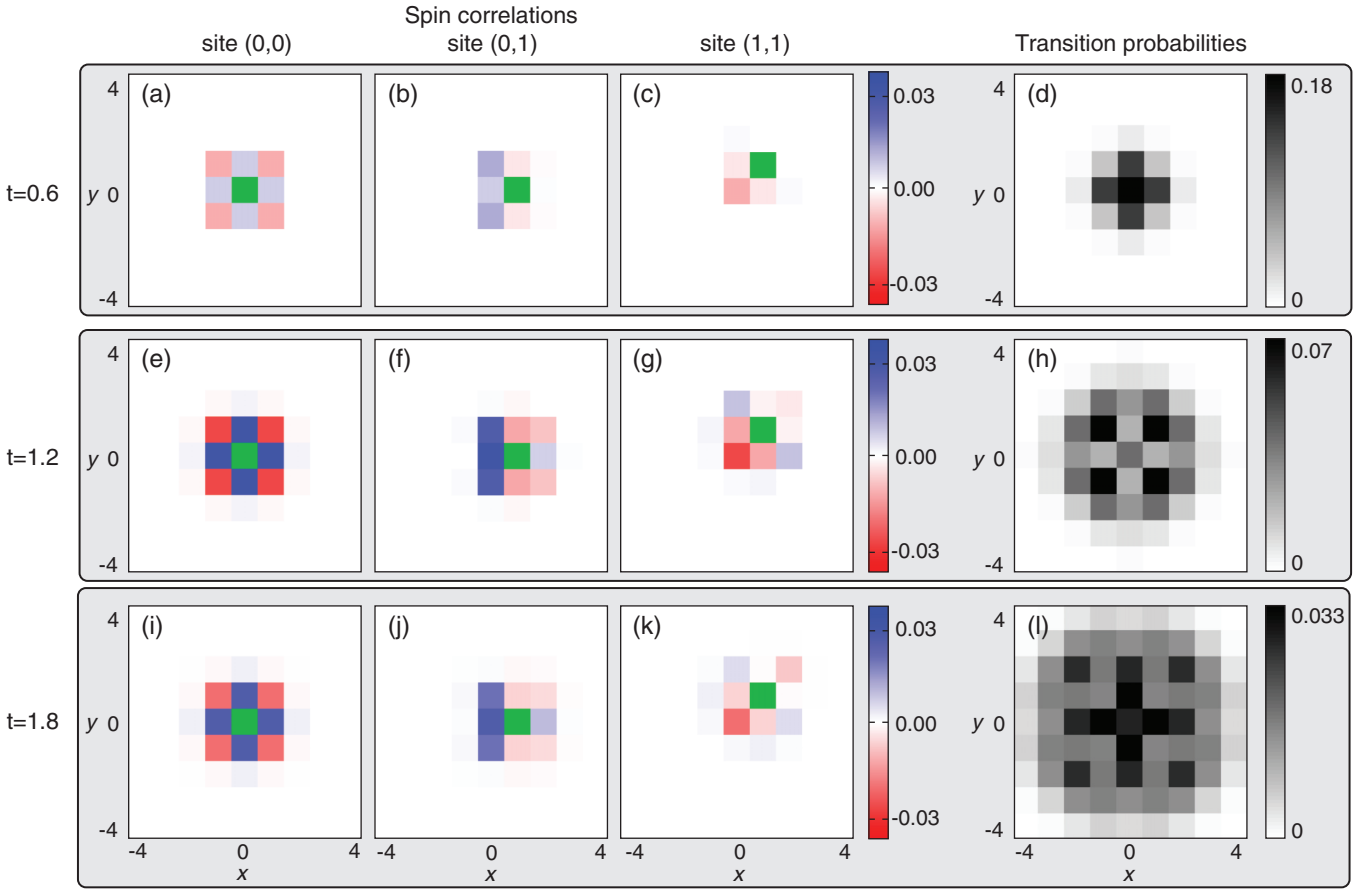

FIG. 2. Induced spin correlations of the hole in a degenerate spin $S = 1/2$ environment in the laboratory frame (left). The reference site j is denoted by green, whereas x and y specify the coordinates of the second site l. The reference site is chosen to be (0,0) for (a), (e), and (i); (0,1) for (b), (f), and (j); and (1,1) for (c), (g), and (k). The probability density of the hole, also discussed by Ref. [25], is exhibited on the right. Results are shown at times $t = 0.6$ (a)–(d), $t = 1.2$ (e)–(h), and $t = 1.8$ (i)–(l) in a spin $S = 1/2$ system.

the time scale of the dynamics. After a propagation time t, the probability of finding the hole at site j is given by $p_j(t) = \langle \hat{c}_j^\dagger \hat{c}_j \rangle(t)$. Here the nonequilibrium average denotes

$$\langle \cdots \rangle(t) = \frac{1}{\mathcal{N}^{M-1}} \mathrm{Tr}(\hat{c}_o e^{i\hat{H}t} \cdots e^{-i\hat{H}t} \hat{c}_o^\dagger),$$

where the trace sums over all possible spin configurations $\mathrm{Tr}(\cdots) = \sum_\Gamma \langle \Gamma | \cdots | \Gamma \rangle$ and the denominator accounts for the of number spin configurations in the environment of M sites.

Whereas the spin environment modifies the propagation of the hole [25], the effect of the hole on the environment can also be observed in the form of dynamical spin correlations, which are the primary focus of this work. The correlations between sites j and l are defined as

$$C_{jl}(t) = \frac{1}{S^2} \langle \hat{S}_j^z \hat{S}_l^z \rangle(t),$$

where $\hat{S}_j^z$ denotes the z component of the spin at that site, and it evaluates to 0 when the hole is at site j. In the initial state, off-diagonal spin correlations $C_{j \neq l}$ are averaged out to zero by thermal fluctuations. Figure 2 shows how the introduction of the hole leads to dynamical correlations at longer times, reaching values as large as 4% near the origin in a system of $S = 1/2$ spins. These correlations appear as the hole extends over the lattice, so that it can build up coherence between the spins surrounding it. In the noninteracting environment, the correlations remain finite at the times available to our simulations. Since the hole cannot create spin flips, the z component of the total spin of the lattice is conserved. This leads to the conservation of the sum of off-diagonal correlations (see Appendix B)

$$\sum_{j \neq l} C_{jl}(t) = 0. \tag{1}$$

Therefore, the appearance of ferromagnetic correlations always need to be accompanied with antiferromagnetic ones and vice versa.

The onset of spin correlations can be understood as follows. In each possible spin background, the hole permutes the spins slightly differently during its dynamics. For instance, locally ferromagnetic environments lead to slightly faster propagation due to interference terms: as the hole has no effect on ferromagnetically aligned spins, any pair of paths interfere. Spin correlations therefore evolve differently in time in each spin environment, and they are not averaged out by thermal fluctuations. Although an experimental realization of the infinite temperature spin background would involve averaging over all initial spin configurations, we estimate that the spin correlations can be observable in existing experimental

setups [50–54] already after a few hundred measurements with a good signal to noise ratio (Appendix A).

III. QUANTUM INTERFERENCE BETWEEN PATHS

Similarly to the famous double-slit experiment [55], the probability of finding the hole at any site is determined from interference between different paths. This leads to interference fringes in the probability density of the hole [25]. The hole's dynamics can be represented in terms of these paths by expanding its time evolution [22,23] as $e^{-i\hat{H}t} = \sum_{n=0}^{\infty} \frac{(-i\,t)^n}{n!}\,\hat{H}^n$. Each power of $\hat{H}$ generates a step of the hole to one of its $z = 4$ neighboring sites. Therefore $\hat{H}^n$ corresponds to a collection of z^n possible hole paths of total length n. During its time evolution, the hole is in the superposition state of all paths. Since the expectation value $\langle\cdots\rangle(t)$ of experimental observables contains both the time evolution operator and its conjugate, we need to expand both of these operators in terms of paths of the hole. These are referred to as forward and backward time evolution paths, respectively. We determine the transition probability $p_j(t)$ by summing over interference terms between all pairs of forward (α) and backward (β) evolution paths ending at site j. In order that two paths can interfere in a given spin environment, the hole needs to end up at the same site along both paths, and they need to produce the same final spin state. As the hole moves along these paths, it generates the permutations $\hat{\pi}_\alpha$ and $\hat{\pi}_\beta$ on the spins. Thus, the transition probability to site j is given by

$$p_j(t) = \sum_{\alpha,\beta} \frac{(-i\,t)^{n_\beta}\,(i\,t)^{n_\alpha}}{n_\beta!\,n_\alpha!}\,\langle\hat{\pi}_\beta^\dagger\hat{\pi}_\alpha\rangle_0,$$

where the average denotes $\langle\cdots\rangle_0 \equiv \langle\cdots\rangle(t=0)$, and n_α and n_β refer to the lengths of the paths α and β. The interference term between paths α and β is thus determined by the combined permutation $\hat{\pi}_\beta^\dagger\hat{\pi}_\alpha = \hat{\pi}_\beta^{-1}\hat{\pi}_\alpha$, which can be generated by the hole moving forward on path α to site j, and then returning to the origin on β. Due to the degeneracy of the spin environment, time-dependent observables cannot be evaluated using ordinary perturbation theory up to finite order in the hopping [56] (see Appendix C). We therefore model the hole's dynamics by sampling its paths using a real-time quantum Monte Carlo algorithm [25,57]. In order to account for the $\frac{t^n}{n!}$ expansion parameter and the large phase space consisting of z^n paths we choose random walk paths of length n from the Poisson distribution $\mathbb{P}_n \propto \frac{(zt)^n}{n!}$ (see Appendix D) [25]. The permutations generated by these paths are stored together with the acquired phase factors i^n and we take all pairs of these paths to evaluate their contributions to the transition probabilities and the spin correlations, as we show in Appendix D. We evaluate interference terms between paths by calculating the thermal average $\langle\cdots\rangle_0$ over all spin states exactly. This allows us to determine the spin correlations to high numerical accuracy, in contrast to earlier approaches [25].

The interference contributions between two paths strongly depend on how the spins are permuted as the hole moves along them. Paths that generate the same permutation of the spin environment $\hat{\pi}_\beta = \hat{\pi}_\alpha$ are referred to as being *equivalent*. These paths restore the original spin configuration at the end of the combined path $\hat{\pi}_\beta^\dagger\hat{\pi}_\alpha = 1$ irrespective of the spin background,

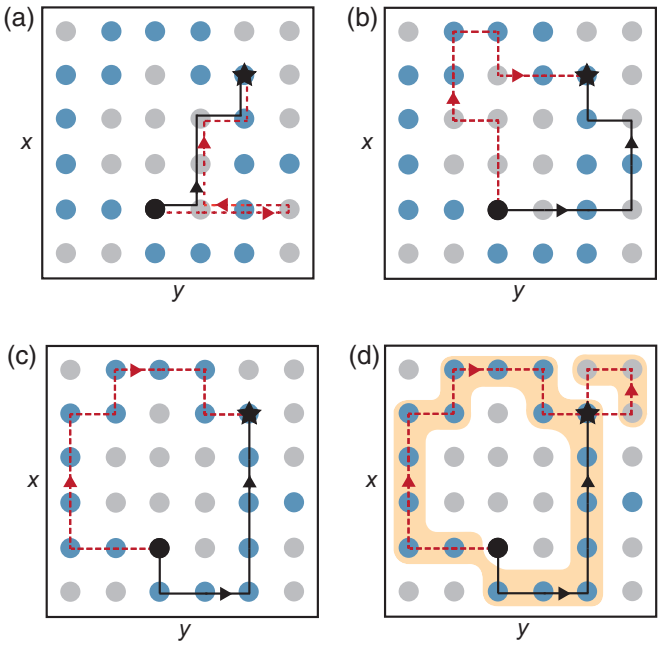

FIG. 3. Interference of different pairs of paths in the same initial spin background. The spin states are denoted by gray (light) and blue (dark) dots. (a) By definition, the two equivalent paths (black full and red dashed lines) permute any spin state identically, making the final spin state the same. Therefore, these paths interfere in any spin background. The inequivalent paths shown in (b) however bring the spin configuration into orthogonal final states, therefore their interference vanishes. In contrast, the paths in (c) and (d) lead to the same final state as these paths permute the spins over locally ferromagnetic regions. The dashed region in (d) shows the permutation cycles generated by the hole moving along the paths. Spin correlations arise from interference between inequivalent paths (b)–(d). However, these contributions vanish in environments of large spin $S \to \infty$. In these systems, the hole's dynamics is determined only by interference between equivalent paths (a).

leading to maximal interference $\langle\hat{\pi}_\beta^\dagger\hat{\pi}_\alpha\rangle_0 = 1$. For example, two paths that only differ in self-retracing components are equivalent [58], as we show in Fig. 3(a). However, more complicated scenarios are also possible. For instance, the path traversing a two-by-two plaquette three times is equivalent to the trivial path, where the hole stays at the origin [59].

Importantly, equivalent paths do not contribute to spin correlations. As they perform the same transformation on the lattice spins, thermal averaging makes the spin correlators vanish. Instead, spin correlations between lattice spins arise from pairs of *inequivalent* paths that have a different effect on the spins, $\hat{\pi}_\beta \neq \hat{\pi}_\alpha$. In these pairs, the combined forward and backward paths always contain loops, such as those shown in Figs. 3(b)–3(d). Depending on the initial spin state, the paths in these pairs often create orthogonal final spin configurations [Fig. 3(b)]. Inequivalent paths can interfere only in specific initial spin states where $\hat{\pi}_\beta^\dagger\hat{\pi}_\alpha$ acts over locally ferromagnetic domains that are restored by the combined permutation [Figs. 3(c) and 3(d)]. These terms thus make the hole's propagation depend on the spin state of the lattice. Similar to the equilibrium Nagaoka effect, the correlations

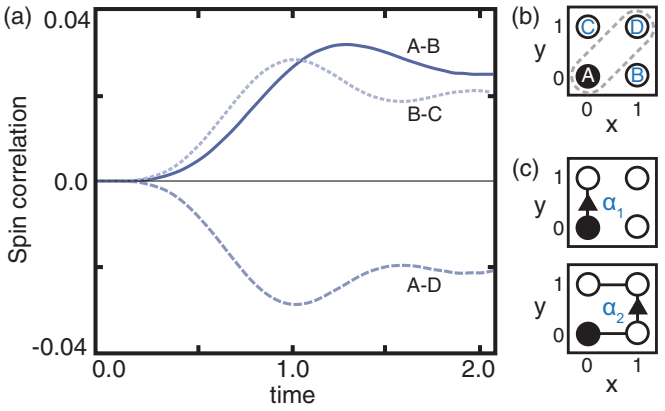

FIG. 4. Time-dependent spin correlations. (a) Correlations between sites neighboring the origin appear gradually and they stay finite during the time scale of our calculation. Results are shown for a spin $S = 1/2$ system. Letters A, B, C, and D in (b) denote sites (0,0),(0,1),(1,0), and (1,1), respectively. Different curves in (a) show correlations between A–B (full line), A–D (dashed line), and B–C (dotted line). (c) Lowest order contributions to A–D correlations [gray dashed circle in (b)] arise from interference between paths encircling the two-by-two plaquette, with the hole ending up at B or at C. Interference between two such paths α_1 (top) and α_2 (bottom) requires nonorthogonality of final spin states. Therefore, all three spins on the plaquette need to be identical.

thus arise from the enhancement of interference terms in ferromagnetic spin domains.

IV. SPIN CORRELATIONS

Figure 4(a) shows that the correlations build up gradually at short times and show slightly oscillating behavior at intermediate times. Whereas correlation between the origin and site (0,1) as well as that between sites (1,0) and (0,1) are ferromagnetic, we find antiferromagnetic correlations between the origin and site (1,1). Figure 2 demonstrates that correlations exist between other sites that are further away from the origin. These correlations appear gradually as the hole approaches the surrounding spins. Within the time scale of our calculations, the correlations stay finite. Their long time behavior remains an open question, which could be addressed experimentally.

To illustrate how spin correlations with different signs emerge, let us consider the lowest order contribution to the correlation between the origin o and site (1,1). As shown in Fig. 4(b), the sites of the plaquette containing these two sites are labeled by letters $A = o$ to $D = (1,1)$, and we thus investigate the spin correlations $C_{AD}(t)$. The hole thus needs to end up at sites $j = B$ or C at time t, otherwise the interference term does not contribute to $C_{AD}(t)$. Due to symmetry, we only need to consider the case when the hole ends up at site C. As we mentioned earlier, spin correlations can only arise from inequivalent pairs of paths. The lowest order such pair ending at site C is shown in the upper and lower panels of Fig. 4(c), and we denote them as α_1 and α_2, respectively. The diagonal matrix elements of the spin correlator vanish after taking the thermal average over all initial spin configurations $\langle \hat{\pi}^\dagger_{\alpha_1} \hat{S}^z_A \hat{S}^z_D \hat{\pi}_{\alpha_1} \rangle_0 = \langle \hat{S}^z_B \rangle_0 \langle \hat{S}^z_C \rangle_0 = 0$, and similarly for path α_2. The interference terms between paths α_1 and α_2, however, yield a nonvanishing contribution for special initial spin states, where α_1 and α_2 result in the same final spin configuration. As the combined effect of the two paths $\hat{\pi}^\dagger_{\alpha_2} \hat{\pi}_{\alpha_1}$ moves all spins to a neighboring site, the interference term is zero unless all three spins are ferromagnetically aligned. In the infinite temperature system, all spins take random values with equal probability $1/\mathcal{N}$. The probability of all three spins taking on the same configuration is given by $\langle \hat{\pi}^\dagger_{\alpha_2} \hat{\pi}_{\alpha_1} \rangle_0 = 1/\mathcal{N}^2$. As interference terms between identical paths average out to zero due to thermal fluctuation, this term determines the sign of correlations

$$C_{AD}(t) = 2\,(it)\frac{(-it)^3}{3!}\langle \hat{\pi}^\dagger_{\alpha_2} \hat{\pi}_{\alpha_1} \rangle_0 \propto -\frac{t^4}{3\mathcal{N}^2}$$

at lowest order, which is negative due to the phase factors acquired by the hole along the two paths. Figure 4(a) shows that the corresponding correlator $C_{AD}(t)$ stays antiferromagnetic at intermediate times as well, whereas $C_{AB}(t)$ and $C_{BC}(t)$ are ferromagnetic.

In order to evaluate spin correlations and transition probabilities up to any order, we consider two arbitrary paths α and β and evaluate their interference $\langle \hat{\pi}^\dagger_\beta \hat{\pi}_\alpha \rangle_0$. Permutations created by longer paths can be more complicated than the one shown in Fig. 4(c) on the two-by-two plaquette. Since longer paths may intersect each other and themselves, the hole may permute different regions of the lattice independently, as we illustrate in Fig. 3(d). In each of these regions, the spins need to be ferromagnetically aligned to ensure that the initial and the final spin state are not orthogonal. However, the individual regions may take on different ferromagnetic states. These regions can be identified by the separate permutation cycles $\mathcal{C}_a$ of the combined permutation $\hat{\pi}^\dagger_\beta \hat{\pi}_\alpha = \Pi_a \mathcal{C}_a$ [60]. The interference term $\langle \hat{\pi}^\dagger_\beta \hat{\pi}_\alpha \rangle_0$ is thus determined by the probability of the spins being ferromagnetically aligned in each cycle,

$$\langle \hat{\pi}^\dagger_\beta \hat{\pi}_\alpha \rangle_0 = \prod_a \frac{1}{\mathcal{N}^{|\mathcal{C}_a|-1}}. \tag{2}$$

Here $|\mathcal{C}_a|$ denotes the number of spins in cycle $\mathcal{C}_a$ and $\mathcal{N} = 2S + 1$ is the number of spin degrees of freedom. This interference term also contributes to the spin correlations between sites within the same ferromagnetic region, as we show in Appendix E. When the spins on sites $\pi^\dagger_\alpha(j)$ and $\pi^\dagger_\alpha(l)$ are within the same ferromagnetic domain, the matrix element $\langle \hat{\pi}^\dagger_\beta S^z_j S^z_l \hat{\pi}_\alpha \rangle$ is simply given by Eq. (2). In contrast, it vanishes for all other combination of sites, as the spin correlations between independent domains average out to zero. We determine both the transition probabilities and spin correlations by Monte Carlo sampling the paths and use Eq. (2) to calculate the interference between each pair of paths (Appendix E).

When the number of spin degrees of freedom is large, it is very unlikely to find locally ferromagnetic regions in an infinite temperature bath. Since interference of inequivalent paths relies on these domains, these contributions vanish in the limit of large spins $S = \infty$, as Eq. (2) shows. The strongest spin correlations can thus be observed in a spin $S = 1/2$ system. Furthermore, the interference term is also exponentially suppressed if the paths permute a large number of spins

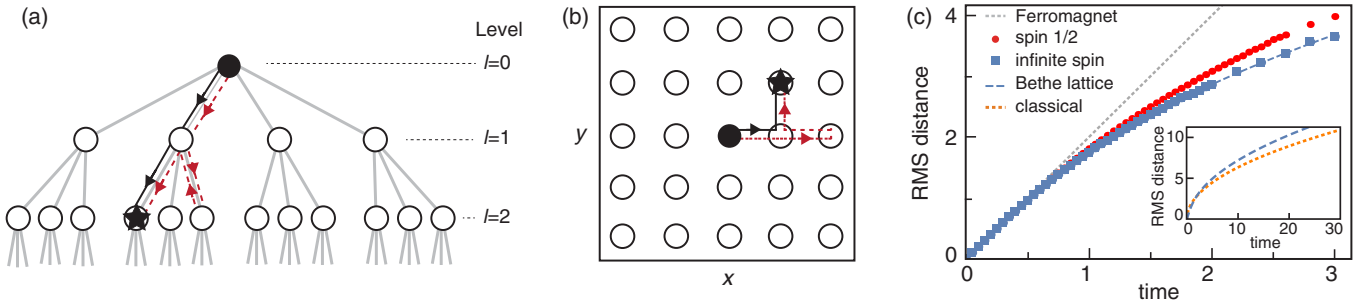

FIG. 5. Bethe lattice model of the hole's dynamics. (a) Bethe lattice of coordination number $z = 4$ with the hole (full black circle) at the origin. Solid and dashed lines indicate two interfering paths and the full black star denotes their endpoint. These paths correspond to random walks of the hole on the two-dimensional lattice shown in (b), with the lattice sites denoted by circles. (c) Comparison of the rms distance of the hole on the Bethe lattice to quantum Monte Carlo results in different spin environments. Blue dashed line corresponds to propagation on the Bethe lattice. The light gray dashed line, red dots, and blue rectangles show results in a ferromagnetic ($S = 0$), a spin $S = 1/2$, and $S = \infty$ degenerate environment, respectively, which have been determined earlier in Ref. [25] for slightly shorter times. Inset: rms distance of the hole on the Bethe lattice (blue dashed line) and for a classical random walk (orange dotted line) at long times.

differently. The largest contribution to spin correlations thus arises from the paths that have almost identical effect on the spins. This explains why the induced spin correlations are localized within a few sites in Fig. 2.

V. HOLE DYNAMICS

The dependence of the hole's propagation on the spin S of the environment has been demonstrated numerically [25]. Here we show that this effect can be attributed to interference between inequivalent paths that are also responsible for the spin correlations in the environment. Furthermore, we give a simple analytic approximation of the hole's dynamics in a large spin $S = \infty$ environment.

In the simplest case of a ferromagnet ($S = 0$), all pairs of paths interfere with a maximal amplitude $\langle \hat{\pi}^\dagger \hat{\pi} \rangle_0 = 1$. As shown in Fig. 5, the resulting propagation is ballistic, and the root mean squared (rms) distance of the hole

$$d_{\mathrm{rms}} = \left(\sum_j p_j \, r_j^2 \right)^{1/2}$$

grows linearly in time, with r_j denoting the distance of site j from the origin. However, the propagation of the hole is slowed down in environments of finite spin, as a result of the suppression of interference terms between inequivalent paths, shown in Eq. (2). Thus, in the $S \to \infty$ limit, only equivalent paths contribute to the dynamics.

In order to gain insight into this limit, we investigate the propagation of the hole on the Bethe lattice [39], shown in Fig. 5(a). The Bethe lattice is a tree graph, with the origin at the root level $l = 0$. Each site has $z = 4$ neighbors that can be identified with left, right, up, and down steps on the two-dimensional lattice. Each random walk on the Bethe lattice can thus be identified with one on the square lattice. The position of the hole on the Bethe lattice keeps full information of its two-dimensional path up to self-retracing components, and two paths interfere if and only if their endpoints are the same. Due to the geometrical constraint imposed by the graph, interfering paths cannot include loops. In particular, the Bethe lattice only allows interference between equivalent paths that are identical except for self-retracing components, see Fig. 5(b). This construction covers most of the phase space of equivalent pairs, which determine the hole's propagation in the $S = \infty$ environment. Therefore, the hole's dynamics in this system is expected to be well approximated by the Bethe lattice construction.

As two interfering paths on the Bethe lattice always permute the spins the same way, the hole's dynamics on the Bethe lattice decouples completely from that of the spins. The hole's propagation therefore becomes a single particle problem that can be solved analytically (Appendix F). This behavior is reminiscent of the physics of spin-charge separation in a one-dimensional lattice [54,61,62], which is equivalent to the Bethe lattice of coordination number $z = 2$. In that case a hole moves coherently in the lattice, while keeping the order of the spins unchanged. Although the spin configuration depends on the hole position, this does not introduce correlations between the spins. In two dimensions, the dynamics on the $z = 4$ Bethe lattice is more subtle. Due to interference between equivalent paths, the average level of the graph grows linearly in time similar to one-dimensional systems (see the Supplemental Material [63]). However, this does not manifest as ballistic propagation on the square lattice. The rms distance of sites on level l of the Bethe lattice becomes

$$d_l = \sqrt{2l - \tfrac{3}{2}(1 - 3^{-l})}, \tag{3}$$

which grows as $d_l \sim \sqrt{2l}$ at large distances (Appendix F). Therefore, instead of ballistic propagation, we find that the hole shows diffusive behavior at long times $d_{\mathrm{rms}} \sim \sqrt{2 D_{\mathrm{Bethe}} t}$, with a diffusion constant

$$D_{\mathrm{Bethe}} \approx 2.73.$$

Thus, the quantum propagation through the random spin environment leads to a diffusion that is faster than that of a classical random walk, with a diffusion constant $D_{\mathrm{cl}} = 2$ (Appendix G).

The rms distance is shown for different models in Fig. 5. We find the usual ballistic propagation in the $S = 0$ ferromagnet, whereas the hole appears to cross over from ballistic to diffusive behavior in the $S > 0$ case at intermediate times

[25]. Figure 5 shows that although the interference between inequivalent paths are small, they lead to faster propagation in the $S = 1/2$ spin environment than in the infinite spin case. This difference is therefore due to the same interference terms that give rise to the spin correlations in the environment. The insight of our work is that the rms distance of the $S = \infty$ model and the Bethe lattice agree within error bars of our simulation, indicating that the behavior of the two models are in very good agreement at short and intermediate times. Therefore we expect that, similar to the Bethe lattice propagation, the hole's dynamics will cross over from ballistic to diffusive behavior in an infinite spin environment.

VI. CONCLUSION

The spin correlations presented in this paper demonstrate a general paradigm of how an originally completely disordered environment can acquire correlations due to quantum interference in the course of nonequilibrium dynamics of a particle. We emphasize that this mechanism is fundamentally different from the interaction-induced correlations in the bath [26–34] and can be observed at infinite temperature of the spin bath. Experimental realization of this phenomenon using ultracold atoms would provide an ideal opportunity for the study of entanglement between a particle and its environment that is usually challenging in other setups due to the fast decoherence in the environment. These experiments could also provide information on the long time dynamics of spin correlation that remains an open question.

Further interesting questions arise about the effect of spin interactions, which appear naturally in experiments with smaller on-site interactions, whether in ultracold atomic or electronic Mott insulators. This would affect spin correlations even in an infinite temperature spin system, as the spin correlations can be decohered by magnetic excitations of the environment. At lower temperatures, the energy cost of permuting spins leads to a strongly renormalized dynamics of the hole [29–31,58,59,64–69]. Understanding this limit, and especially the interplay of multiple holes with the environment, could also lead to a better understanding of the role of doping in the cuprate phase diagram [24,40,41,64,68–70].

ACKNOWLEDGMENTS

We thank J. Carlström, N. Prokof'ev, G. Zaránd, and J. van den Brink for enlightening discussions. The authors acknowledge support from Harvard-MIT CUA, NSF Grant No. DMR-1308435, AFOSR Quantum Simulation MURI, AFOSR Grant No. FA9550-16-1-0323, the Moore Foundation, the Harvard Quantum Optics Center, and the Swiss National Foundation. I.L. was supported by the Hungarian research Grant OTKA No. K105149 and No. SNN118028.

APPENDIX A: MODELING EXPERIMENTAL NOISE

Quantum gas microscope experiments take individual measurements of the spin configuration on the lattice, and the thermal average is evaluated by averaging over many experimental runs. In the infinite temperature spin environment, each spin takes on one of the $\mathcal{N}$ spin states with equal probability. Therefore, after K measurements, the experimental noise of the spin correlations is proportional to $K^{-1/2}$. In order to reduce experimental noise, one can also make use of the reflection and fourfold rotation symmetries of the two-dimensional lattice, and average the spin correlations according to these symmetries. We illustrate the role of experimental noise, by starting simulations from K random initial spin configurations $|\Gamma_i\rangle$ in a spin $S = 1/2$ system. Instead of evaluating the spin average exactly as we did in the main text, we average over only these configurations $C_{jl}(t) \approx \frac{1}{K}\sum_{i=1}^{K}\langle\Gamma_i|c_o\, e^{iHt}\, S_j^z S_l^z\, e^{-iHt} c_o^\dagger|\Gamma_i\rangle$. Figure 6 shows the spin correlations of the hole after symmetry averaging. We obtain good signal-to-noise ratio already after $K = 500$ runs. The details of the quantum Monte Carlo procedure performing finite number of spin averaging is described in Appendix D.

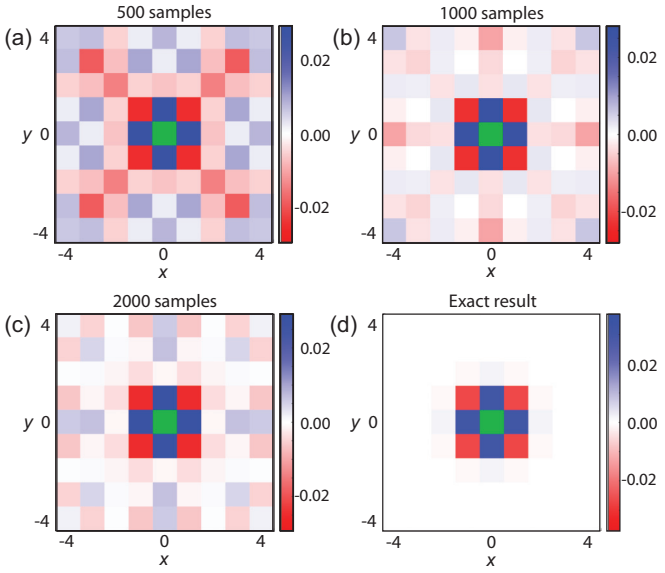

FIG. 6. Simulation of spin correlations after a finite number of experimental runs. Spin correlations $C_{jl}(t)$ measured after time evolution of $t = 1.2$ in a spin $S = 1/2$ system. The reference site j is chosen to be the origin, whereas the coordinates of the lattice correspond to site l. The spin correlations are averaged over the fourfold rotational symmetry and over all reflection symmetries of the lattice to obtain better signal to noise ratio. (a)–(d) Averaging over 500, 1000, 2000, and all initial spin states, respectively.

We mention furthermore that quantum gas experiments are often initialized with approximately the same total magnetization in each experimental run, which constrains the total magnetization of the system. In this work we assume that the infinite temperature spin bath realizes all possible spin configurations with equal probability, and we neglect any constraint on the total magnetization. This assumption is a good approximation if the hole's dynamics is studied in a region that is small compared to the overall size of the system, as the constraint on the total magnetization of the entire system will not significantly affect the magnetization of the measurement region.

APPENDIX B: EFFECT OF SPIN CONSERVATION.

Since the hole cannot create spin flips, the total spin $S^z_{\rm tot} = \sum_j S^z_j$ is conserved. The time dependence of the square of this

operator can be expressed in terms of spin correlations,

$$\frac{1}{S^2}\,\langle c_o^\dagger\, e^{iHt}\,(S^z_{\rm tot})^2\, e^{-iHt}\, c_o^\dagger\rangle = \sum_j C_{jj}(t) + \sum_{j\neq l} C_{jl}(t).$$

The diagonal spin correlations are simply given by $C_{jj}(t) = 1 - p_j(t)$, the sum of these correlations is thus constant $\sum_j C_{jj}(t) = M - 1$, where M is the number of sites of the system. We thus find that the sum of off-diagonal spin correlations is conserved. Since it is zero in the initial state, we arrive at the sum rule in Eq. (1).

APPENDIX C: BREAKDOWN OF PERTURBATION THEORY AT FINITE ORDERS

Due to the degeneracy of the spin environment, perturbation theory of the time evolution up to any finite order in time breaks down, as we discussed in the main text [56]. Therefore, the expansion of the time evolution $e^{-iHt} = \sum_{n=0}^{\infty} \frac{(-it)^n}{n!} H^n$ needs to be summed up to infinite order. We perform the summation numerically by sampling the paths of the hole using a quantum Monte Carlo procedure [25]. This method falls into the family of stochastic series expansion quantum Monte Carlo techniques [71]. As we discussed in the main text, the paths are chosen according to a Poisson distribution of mean zt, where $z = 4$ is the coordination number of the lattice. Figure 7(a) shows the distribution of paths at different times. Whereas the average length of paths is zt, one needs to take into account significantly shorter and longer paths as well to ensure convergence. Truncating the series at any finite order, and thereby neglecting the contribution of long paths leads to the divergence of the time evolution of the spin correlations $C_{jl}(t)$ at long enough times, as we show in Fig. 7(b).

APPENDIX D: REAL-TIME QUANTUM MONTE CARLO ALGORITHM

We sample the time evolution operator using stochastic series expansion quantum Monte Carlo [25,71]. At the beginning of the simulation, we generate of the order of 2×10^8 random walk paths. The permutations generated by these paths are binned, and their phase factors i^n are added. The $\frac{t^n}{n!}$ amplitudes are taken into account by sampling the path lengths n according to a Poisson distribution

$$\mathbb{P}_n = \frac{(zt)^n}{n!} e^{-zt}.$$

The resulting amplitudes λ are stored together with the corresponding permutations $\hat\pi$ as pairs $(\lambda,\hat\pi)$. We take all possible combinations of forward $(\lambda_\alpha,\hat\pi_\alpha)$ and backward $(\lambda_\beta,\hat\pi_\beta)$ time evolution bins. We evaluate the many-body trace associated with each pair exactly, using Eq. (2). We add the interference contribution $\lambda^*_\beta \lambda_\alpha \langle \hat\pi^\dagger_\beta \hat\pi_\alpha\rangle$ to the histogram of the transition probabilities $\tilde p_j(t)$ and that of spin correlations $\tilde C_{jl}(t)$ for appropriate sites j and l. At the end of the simulation, we normalize the histograms $\tilde p_j(t)$ and $\tilde C_{jl}(t)$ by dividing them by $\sum_j \tilde p_j(t)$.

Evaluating the infinite temperature spin averages exactly allows us to sample the spin correlation with very small noise as compared to performing numerical averaging over different spin configurations [25]. However, around time $t \sim 1.8$, the phase space of probable paths becomes significantly larger than the number of our path samples. Since the number of path bins L also becomes very large, calculating the interference contributions of all the $L \times L$ pairs of path bins becomes impractical. Therefore, at longer times $2 < t < 3$, we calculate the rms distance using a slightly modified version of the algorithm of Ref. [25], but with different set of forward and backward paths. Although this method provides noisy spin correlation data, it determines rms distance at longer times very accurately, and requires only of the order of L steps.

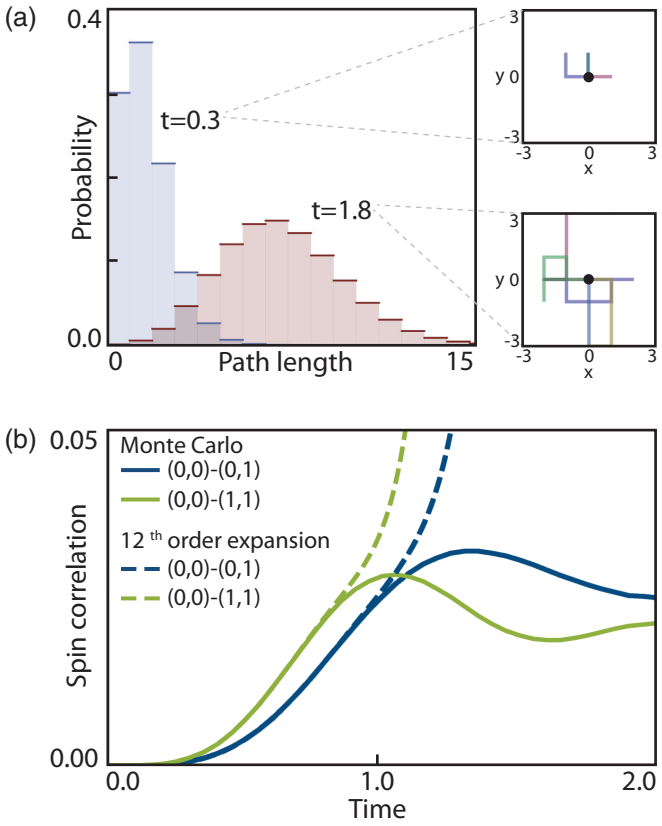

FIG. 7. Quantum Monte Carlo versus finite order perturbation theory. (a) Distribution of the path lengths in the quantum Monte Carlo algorithm at different times. The panels show five different examples of random paths at these times. (b) Comparison of spin correlations results using perturbation theory to 12th order in time (dashed lines) versus the quantum Monte Carlo procedure presented in the main text (full lines). Blue (dark) and green (light) lines denote correlations between sites (0,0)–(0,1) and (0,0)–(1,1), respectively.

Throughout this paper, we sample the forward e^{-iHt} and backward e^{iHt} time evolution paths independently, in contrast to earlier approaches [25]. The independent sampling becomes important at times longer than $t \sim 1.8$, when the phase space of paths becomes so large that the quantum Monte Carlo procedure can sample it only sparsely. At these times, two typical paths α and β will in general enclose large loops. According to Eq. (2), their interference $\langle \hat\pi^\dagger_\beta \hat\pi_\alpha\rangle_0$ is exponentially small.

Choosing the forward and backward time evolution paths from the same sample would lead to large systematic errors. In contrast to independent sampling, this procedure would

oversample those cases when the forward and backward paths are identical. These pairs have an interference of $\langle \hat{\pi}_\alpha^\dagger \hat{\pi}_\alpha \rangle_0 = 1$, in contrast to the typically exponentially small interference of nonidentical pairs. Therefore, the pairs consisting of identical paths would overwhelm contributions from nonidentical paths, leading to incorrect results. By sampling the forward and backward evolution paths independently, these errors can be avoided.

APPENDIX E: INTERFERENCE CONTRIBUTION TO SPIN CORRELATIONS

The contribution of paths α and β to the spin correlations $C_{jl}(t)$ is given by $\frac{(-it)^{n_\beta}\,(it)^{n_\alpha}}{n_\beta!\,n_\alpha!}\,\langle \hat{\pi}_\beta^\dagger S_j^z S_l^z \hat{\pi}_\alpha \rangle$. Here n_β and n_α denote the lengths of these paths. The nonorthogonality of the initial and the final spin states requires each permutation cycle of the combined path $\hat{\pi}_\beta^\dagger \hat{\pi}_\alpha$ to be ferromagnetic. Therefore, if the spins on sites $j' = \pi_\alpha^\dagger(j)$ and $l' = \pi_\alpha^\dagger(l)$ are in the same permutation cycle, the above expectation value becomes

$$\langle \hat{\pi}_\beta^\dagger S_j^z S_l^z \hat{\pi}_\alpha \rangle = \langle \hat{\pi}_\beta^\dagger \hat{\pi}_\alpha S_{j'}^z S_{l'}^z \rangle = \frac{S(S+1)}{3} \langle \hat{\pi}_\beta^\dagger \hat{\pi}_\alpha \rangle.$$

The S dependent prefactor in the previous equation arises from averaging the spin operators over all $(2S+1)$ possible ferromagnetic spin configurations. For all other pairs of sites, the spins are independent, and the expectation value $\langle \hat{\pi}_\beta^\dagger S_j^z S_l^z \hat{\pi}_\alpha \rangle$ thus averages out to zero in the infinite temperature spin environment.

APPENDIX F: PROPAGATION ON THE BETHE LATTICE

The hole's propagation on the Bethe lattice can be solved analytically, as we show in the Supplemental Material [63]. Here we present a shorter, recursive solution. Expanding the time evolution in terms of random walks, we find that the wave function of the hole at level l is given by

$$\psi_l(t) = \frac{1}{M_l} \sum_{n=0}^{\infty} \frac{(-izt)^n}{n!} \rho_{n,l},$$

where M_l denotes the number of sites on level l of the Bethe lattice, with $M_l = 1/[z\,(z-1)^{l-1}]$ for $l \geqslant 1$, and $M_0 = 1$. The matrix $\rho_{n,l}$ denotes the probability that a random walk path of length n ends up at level l. These probabilities can be determined using simple recurrence relations. At all levels $l \geqslant 1$, the probability of taking a step one level down on the graph is $3/4$ and taking a step up has a probability $1/4$. At the origin, the walker goes to level $l = 1$ with probability 1. This leads to the following recurrence relations:

$$\rho_{n+1,\,l} = \tfrac{3}{4}\,\rho_{n,\,l-1} + \tfrac{1}{4}\,\rho_{n,\,l+1}$$

for $l \geqslant 2$, and for levels $l = 0, 1$ we get

$$\rho_{n+1,\,1} = \rho_{n,\,0} + \tfrac{1}{4}\rho_{n,\,2},$$
$$\rho_{n,\,0} = \tfrac{1}{4}\rho_{n,\,1}.$$

We solve these equations iteratively, starting from the initial condition $\rho_{0,l} = \delta_{0,l}$.

We determine the rms distance d_l of sites on level l, using an iterative procedure. When mapping the sites at level l of the Bethe lattice to the square lattice, we get the end points of all possible random walks of length l, involving no self-retracing components. In order to calculate the rms distance for the end points of such random walks, we write down a recurrence relation between d_l^2 and d_{l-1}^2. Let (x_l, y_l) denote the hole's displacement in its lth step. We can assume without the loss of generality that the first step was taken to the right. The rms distance of the endpoint can be written as

$$d_l^2 = d_{l-1}^2 + 2\overline{x}_{l-1} + 1,$$

where $\overline{x}_{l-1}$ denotes the average number of right steps in the remaining path. This quantity is nonzero since the left-right symmetry of the walk is broken due to the initial step. However, after the first time the hole moves in the up or down direction, the left-right symmetry of the model is restored, and the remaining part of the path does not contribute to $\overline{x}_{l-1}$. The probability of taking n steps to the right, and then an up or down step is given by $(1/3)^n\,(2/3)$. Summing up the series for all $n < l-1$, and adding the probability of taking all remaining $l-1$ steps to the right, $(1/3)^{l-1}$, leads to $\overline{x}_{l-1} = (1 - 3^{-(l-1)})/2$. We thus obtain the recurrence relation

$$d_l^2 = d_{l-1}^2 + 2 - 3^{-(l-1)},$$

which can be solved exactly, yielding Eq. (3).

APPENDIX G: COMPARISON WITH CLASSICAL RANDOM WALKS

We compare the quantum dynamics of the hole to that of a classical particle performing Brownian motion. With the particle starting from the origin, its time evolution is governed by a transition rate matrix, assigning the transition rate 1 to each of its neighboring sites i and j. The probability distribution of the particle thus follows a classical diffusion equation, with a diffusion constant $D_{\rm cl} = 2$.

[1] J. R. Friedman, V. Patel, W. Chen, S. Tolpygo, and J. E. Lukens, Nature (London) **406**, 43 (2000).

[2] L. Hofstetter, S. Csonka, J. Nygård, and C. Schönenberger, Nature (London) **461**, 960 (2009).

[3] M. Andrews, C. Townsend, H.-J. Miesner, D. Durfee, D. Kurn, and W. Ketterle, Science **275**, 637 (1997).

[4] R. Simmonds, A. Marchenkov, E. Hoskinson, J. Davis, and R. Packard, Nature (London) **412**, 55 (2001).

[5] J. K. Chin, D. Miller, Y. Liu, C. Stan, W. Setiawan, C. Sanner, K. Xu, and W. Ketterle, Nature (London) **443**, 961 (2006).

[6] M. Blume and J. Hubbard, Phys. Rev. B **1**, 3815 (1970).

[7] M. Chertkov and I. Kolokolov, Phys. Rev. B **49**, 3592 (1994).

[8] S. Lovesey, E. Engdahl, A. Cuccoli, V. Tognetti, and E. Balcar, J. Phys.: Condens. Matter **6**, L521 (1994).

[9] G. S. Engel, T. R. Calhoun, E. L. Read, T.-K. Ahn, T. Mančal, Y.-C. Cheng, R. E. Blankenship, and G. R. Fleming, Nature (London) **446**, 782 (2007).

[10] E. Collini, C. Y. Wong, K. E. Wilk, P. M. Curmi, P. Brumer, and G. D. Scholes, Nature (London) **463**, 644 (2010).

[11] G. Panitchayangkoon, D. Hayes, K. A. Fransted, J. R. Caram, E. Harel, J. Wen, R. E. Blankenship, and G. S. Engel, Proc. Natl. Acad. Sci. **107**, 12766 (2010).
[12] T. Ritz, S. Adem, and K. Schulten, Biophys. J. **78**, 707 (2000).
[13] L. Turin, Chem. Senses **21**, 773 (1996).
[14] M. A. Nielsen and I. Chuang, *Quantum Computation and Quantum Information*, 10th ed. (Cambridge University Press, Cambridge, 2010).
[15] N. V. Prokof'ev and P. C. E. Stamp, Phys. Rev. A **74**, 020102 (2006).
[16] A. Morello, P. C. E. Stamp, and I. S. Tupitsyn, Phys. Rev. Lett. **97**, 207206 (2006).
[17] K. S. Novoselov, Z. Jiang, Y. Zhang, S. Morozov, H. L. Stormer, U. Zeitler, J. Maan, G. Boebinger, P. Kim, and A. K. Geim, Science **315**, 1379 (2007).
[18] S. Lloyd, J. Phys.: Conf. Ser. **302**, 012037 (2011).
[19] W. H. Zurek, Phys. Today **44**, 36 (1991).
[20] R. Jördens, N. Strohmaier, K. Günter, H. Moritz, and T. Esslinger, Nature (London) **455**, 204 (2008).
[21] C. Hofrichter, L. Riegger, F. Scazza, M. Höfer, D. R. Fernandes, I. Bloch, and S. Fölling, Phys. Rev. X **6**, 021030 (2016).
[22] Y. Nagaoka, Solid State Commun. **3**, 409 (1965).
[23] Y. Nagaoka, Phys. Rev. **147**, 392 (1966).
[24] A. Auerbach, *Interacting Electrons and Quantum Magnetism* (Springer Science & Business Media, New York, 2012).
[25] J. Carlström, N. Prokof'ev, and B. Svistunov, Phys. Rev. Lett. **116**, 247202 (2016).
[26] L. D. Landau, Phys. Z. Sowjetunion **3**, 644 (1933).
[27] H. Fröhlich, Adv. Phys. **3**, 325 (1954).
[28] A. S. Mishchenko, N. V. Prokof'ev, A. Sakamoto, and B. V. Svistunov, Phys. Rev. B **62**, 6317 (2000).
[29] Q. Zhang and K. B. Whaley, Phys. Rev. B **43**, 11062 (1991).
[30] A. S. Mishchenko, N. V. Prokof'ev, and B. V. Svistunov, Phys. Rev. B **64**, 033101 (2001).
[31] S. R. White and I. Affleck, Phys. Rev. B **64**, 024411 (2001).
[32] Y. E. Shchadilova, R. Schmidt, F. Grusdt, and E. Demler, Phys. Rev. Lett. **117**, 113002 (2016).
[33] N. B. Jørgensen, L. Wacker, K. T. Skalmstang, M. M. Parish, J. Levinsen, R. S. Christensen, G. M. Bruun, and J. J. Arlt, Phys. Rev. Lett. **117**, 055302 (2016).
[34] M.-G. Hu, M. J. Van de Graaff, D. Kedar, J. P. Corson, E. A. Cornell, and D. S. Jin, Phys. Rev. Lett. **117**, 055301 (2016).
[35] D. Mozyrsky and V. Privman, J. Stat. Phys. **91**, 787 (1998).
[36] G. Gangopadhyay, M. S. Kumar, and S. Dattagupta, J. Phys. A **34**, 5485 (2001).
[37] N. Prokof'ev and P. Stamp, Rep. Prog. Phys. **63**, 669 (2000).
[38] W. Unruh, Philos. Trans. R. Soc. London Sect. A **370**, 4454 (2012).
[39] M. Ostilli, Physica A **391**, 3417 (2012).
[40] P. A. Lee, N. Nagaosa, and X.-G. Wen, Rev. Mod. Phys. **78**, 17 (2006).
[41] S. Sachdev, *Quantum Phase Transitions* (Wiley Online Library, New York, 2007).
[42] J. B. Sokoloff and A. Widom, Phys. Rev. Lett. **35**, 673 (1975).
[43] G. Montambaux, M. Heritier, and P. Lederer, J. Low Temp. Phys. **47**, 39 (1982).
[44] P. Kumar and N. S. Sullivan, Phys. Rev. Lett. **55**, 963 (1985).
[45] P. Kumar and N. S. Sullivan, Phys. Rev. B **35**, 3162 (1987).
[46] A. G. Lebed, *The Physics of Organic Superconductors and Conductors* (Springer, New York, 2008), Vol. 110.
[47] Y. Tokura and Y. Tomioka, J. Magn. Magn. Mater. **200**, 1 (1999).
[48] H. Röder, J. Zang, and A. R. Bishop, Phys. Rev. Lett. **76**, 1356 (1996).
[49] M. Greiner, O. Mandel, T. Esslinger, T. W. Hänsch, and I. Bloch, Nature (London) **415**, 39 (2002).
[50] D. Greif, M. F. Parsons, A. Mazurenko, C. S. Chiu, S. Blatt, F. Huber, G. Ji, and M. Greiner, Science **351**, 953 (2016).
[51] C. Weitenberg, M. Endres, J. F. Sherson, M. Cheneau, P. Schauss, T. Fukuhara, I. Bloch, and S. Kuhr, Nature (London) **471**, 319 (2011).
[52] M. Endres, M. Cheneau, T. Fukuhara, C. Weitenberg, P. Schauß, C. Gross, L. Mazza, M. C. Bañuls, L. Pollet, I. Bloch *et al.*, Science **334**, 200 (2011).
[53] L. W. Cheuk, M. A. Nichols, K. R. Lawrence, M. Okan, H. Zhang, and M. W. Zwierlein, Phys. Rev. Lett. **116**, 235301 (2016).
[54] T. A. Hilker, G. Salomon, F. Grusdt, A. Omran, M. Boll, E. Demler, I. Bloch, and C. Gross, arXiv:1702.00642.
[55] R. P. Feynman, R. B. Leighton, M. Sands, and R. B. Lindsay, *The Feynman Lectures on Physics, Vol. 3: Quantum Mechanics* (Addison-Wesley, Reading, Mass., 1965).
[56] D. M. Esterling and R. V. Lange, Phys. Rev. B **1**, 2231 (1970).
[57] D. Handscomb, in *Mathematical Proceedings of the Cambridge Philosophical Society* (Cambridge University Press, Cambridge, 1962), Vol. 58, pp. 594–598.
[58] W. F. Brinkman and T. M. Rice, Phys. Rev. B **2**, 1324 (1970).
[59] S. A. Trugman, Phys. Rev. B **37**, 1597 (1988).
[60] H. F. Jones, *Groups, Representations and Physics* (CRC, Boca Raton, FL, 1998).
[61] M. Ogata and H. Shiba, Phys. Rev. B **41**, 2326 (1990).
[62] H. V. Kruis, I. P. McCulloch, Z. Nussinov, and J. Zaanen, Phys. Rev. B **70**, 075109 (2004).
[63] See Supplemental Material at http://link.aps.org/supplemental/10.1103/PhysRevB.96.014303 for the analytical solution of the hole's propagation on the Bethe lattice.
[64] L. N. Bulaevski, E. L. Nagaev, and D. I. Khomskii, Sov. J. Exp. Theor. Phys. **27**, 836 (1968).
[65] S. Schmitt-Rink, C. M. Varma, and A. E. Ruckenstein, Phys. Rev. Lett. **60**, 2793 (1988).
[66] C. L. Kane, P. A. Lee, and N. Read, Phys. Rev. B **39**, 6880 (1989).
[67] M. Mierzejewski, L. Vidmar, J. Bonča, and P. Prelovšek, Phys. Rev. Lett. **106**, 196401 (2011).
[68] J. Bonča, M. Mierzejewski, and L. Vidmar, Phys. Rev. Lett. **109**, 156404 (2012).
[69] S. Dal Conte, L. Vidmar, D. Golež, M. Mierzejewski, G. Soavi, S. Peli, F. Banfi, G. Ferrini, R. Comin, B. M. Ludbrook *et al.*, Nat. Phys. **11**, 421 (2015).
[70] B. S. Shastry, H. R. Krishnamurthy, and P. W. Anderson, Phys. Rev. B **41**, 2375 (1990).
[71] A. W. Sandvik and J. Kurkijärvi, Phys. Rev. B **43**, 5950 (1991).